JACS
JOURNAL OF THE AMERICAN CHEMICAL SOCIETY
Communication
pubs.acs.org/JACS

Fabrication of Efficient Low-Bandgap Perovskite Solar Cells by Combining Formamidinium Tin Iodide with Methylammonium Lead Iodide

Weiqiang Liao,[†,‡,#] Dewei Zhao,[*,†,#] Yue Yu,[†] Niraj Shrestha,[†] Kiran Ghimire,[†] Corey R. Grice,[†] Changlei Wang,[†,⊥] Yuqing Xiao,[⊥] Alexander J. Cimaroli,[†] Randy J. Ellingson,[†] Nikolas J. Podraza,[†] Kai Zhu,[§] Ren-Gen Xiong,[*,‡] and Yanfa Yan[*,†]

[†]Department of Physics and Astronomy and Wright Center for Photovoltaics Innovation and Commercialization, The University of Toledo, Toledo, Ohio 43606, United States

[‡]Ordered Matter Science Research Center, Southeast University, Nanjing 211189, China

[⊥]Key Laboratory of Artificial Micro/Nano Structures of Ministry of Education, School of Physics and Technology, Wuhan University, Wuhan 430072, China

[§]Chemistry and Nanoscience Center, National Renewable Energy Laboratory, Golden, Colorado 80401, United States

Supporting Information

ABSTRACT: Mixed tin (Sn)−lead (Pb) perovskites with high Sn content exhibit low bandgaps suitable for fabricating the bottom cell of perovskite-based tandem solar cells. In this work, we report on the fabrication of efficient mixed Sn−Pb perovskite solar cells using precursors combining formamidinium tin iodide ($FASnI_3$) and methylammonium lead iodide ($MAPbI_3$). The best-performing cell fabricated using a $(FASnI_3)_{0.6}(MAPbI_3)_{0.4}$ absorber with an absorption edge of ∼1.2 eV achieved a power conversion efficiency (PCE) of 15.08 (15.00)% with an open-circuit voltage of 0.795 (0.799) V, a short-circuit current density of 26.86(26.82) mA/cm^2, and a fill factor of 70.6(70.0)% when measured under forward (reverse) voltage scan. The average PCE of 50 cells we have fabricated is 14.39 ± 0.33%, indicating good reproducibility.

Organic−inorganic lead (Pb) halide perovskite solar cells (PVSCs) are a promising photovoltaic technology for low-cost solar energy conversion due to their low-temperature solution process and high power conversion efficiencies (PCEs). Remarkable progress on the PCE has been demonstrated in the past few years, with a current record PCE of 22.1%.[1] Further improvement on PCEs is highly desirable for cost-reduction and potential deployment of this new photovoltaic technology. The most promising approach to push the PCEs beyond the Shockley−Queisser limit for single-junction solar cells is to fabricate perovskite based tandem solar cells. Methylammonium (MA) and formamidinium (FA) Pb halide perovskites have impressive bandgap tunability. By varying the bromide (Br):iodide (I) ratio, Pb perovskites with mixed halides have exhibited bandgaps in the range of 1.58−2.2 eV,[2] suitable for the top cell in tandem solar cells. By tuning the tin (Sn):Pb ratio, mixed Sn and Pb perovskites can exhibit bandgaps from 1.17 to 1.55 eV, suitable for the bottom cell in tandem solar cells.[3] Therefore, halide perovskites present an unusual opportunity for fabricating ultrahigh efficiency and low-cost polycrystalline tandem cells using low-temperature solution processes.

So far, most reported perovskite-based tandem solar cells used wide-bandgap perovskite cells as the top cell and low-bandgap nonperovskite solar cells as the bottom cell, including silicon (Si), copper indium gallium selenide (CIGS), and polymer based solar cells.[2,4] There are only limited efforts on fabricating perovskite−perovskite tandem cells.[4c,d] In these attempts, the perovskite absorbers used for the bottom cells did not have low-bandgaps, which fundamentally limits the PCEs of tandem solar cells. The lack of fabricating efficient all-perovskite tandem solar cells is primarily due to the largely lagged progress on making efficient low bandgap PVSCs. In contrast, the development of efficient wide-bandgap PVSCs has progressed very well.[2,5] Whereas Snaith and co-workers have recently shown a 17% PCE for mixed cation lead mixed halide perovskites with a reported bandgap of ∼1.74 eV,[2] the highest PCE of low-bandgap mixed Sn−Pb PVSCs has still remained at 7.37%, which was achieved by Kanatzidis' group in 2014 with $MASn_{0.75}Pb_{0.25}I_3$ having a bandgap of 1.17 eV.[3b] Jen and co-workers showed that in order to improve the PCE of mixed Sn−Pb PVSCs, higher Pb content was needed.[6] A PCE of 9.77% was achieved for a $MASn_{0.15}Pb_{0.85}I_{3-y}Cl_y$ (bandgap of 1.38 eV) PVSC. A further enhanced PCE of 14.2% for $MA_{0.5}FA_{0.5}Pb_{0.75}Sn_{0.25}I_3$ PVSC (bandgap of 1.33 eV) has been recently presented.[7] However, such a relatively large bandgap is not ideal for tandem cell applications.

The slow progress on improving the PCE of mixed Sn−Pb PVSCs may be attributed to the facile oxidation of Sn^{2+} to Sn^{4+}. This instability is known to cause high carrier density and nonuniform perovskite films, which are undesirable for high performance cells. Recent progress on fabricating Pb-free Sn PVSCs has provided some insights for potentially overcoming these issues. First, it was reported that $FASnI_3$ is more stable

Received: August 11, 2016
Published: September 13, 2016

DOI: 10.1021/jacs.6b08337
J. Am. Chem. Soc. 2016, 138, 12360−12363

than $MASnI_3$.[8] Seok and co-workers reported a PCE of 4.8% for a $FASnI_3$ PVSC.[9] Second, Kanatzidis and co-workers and Mathews and co-workers have reported that tin fluoride (SnF_2) additives can effectively suppress the oxidization of Sn^{2+} and reduce the hole density in the resulting films, and therefore improve the PCEs of Sn PVSCs.[10] Third, it was noticed that the lithium (Li) and/or cobalt (Co) salts used as dopants in organic hole selective layers (HSLs) may damage Sn perovskites. These important insights should be taken into account when developing efficient mixed Sn−Pb PVSCs with low bandgaps.

In this work, we used a new precursor and inverted cell structure to avoid the aforementioned issues associated with the incorporation of Sn, which enabled us to deposit high quality mixed Sn−Pb thin films and to fabricate efficient low-bandgap mixed Sn−Pb PVSCs. Unlike previous reports using MA with Sn and Pb iodides, our new precursor combines a $FASnI_3$ precursor with a $MAPbI_3$ precursor, taking the advantages of our recent success on fabricating efficient Pb-free Sn PVSCs and Pb-based PVSCs.[11] The composition of the thin films is controlled by the molar ratio of $MAPbI_3$ to $FASnI_3$ precursors, giving a formula of $(FASnI_3)_{1-x}(MAPbI_3)_x$. The lowest bandgap, ~1.2 eV, was obtained with x = 0.4. We have fabricated 50 solar cells with an active area of 0.12 cm^2 using $(FASnI_3)_{0.6}(MAPbI_3)_{0.4}$ absorbers and achieved an average PCE of 14.39 ± 0.33% with an average open-circuit voltage (V_{oc}) of 0.800 ± 0.009 V, an average short-circuit current density (J_{sc}) of 26.33 ± 0.37 mA/cm^2, and an average fill factor (FF) of 68.3 ± 1.2% when measured under forward voltage scan, revealing good reproducibility. The devices showed very little hysteresis in photocurrent−voltage (J−V). The best performing cell showed a PCE of 15.08 (15.00)% with a V_{oc} of 0.795 (0.799) V, a J_{sc} of 26.86 (26.82) mA/cm^2, and a FF of 70.6 (70.0)% when measured under forward (reverse) voltage scan. The improvement in PCE from 7.37% to 15.0% represents a significant advance over all reported PVSCs with similar bandgaps and paves a way for fabricating efficient all-perovskite tandem solar cells.

Figure 1a shows the steps of the formation of our precursor used for one-step deposition of mixed Sn−Pb perovskite thin films, combining the $FASnI_3$ precursor with the $MAPbI_3$ precursor at different molar ratios. Following the recipe reported by Kanatzidis' group, we used a DMSO-based cosolvent to dissolve $FASnI_3$ and $MAPbI_3$, which are known to give good film morphology. The $FASnI_3$ solution contains 10 mol % SnF_2 additive, which is necessary for suppressing the carrier concentration of Sn perovskite thin films.[12] The mixed Sn−Pb perovskite thin films were deposited by spin-coating the precursor composed of $FASnI_3$ precursor and $MAPbI_3$ precursor with desirable molar ratios. After a diethyl ether dripping, the perovskite thin films were annealed at 100 °C for 5 min. The morphology of $(FASnI_3)_{1-x}(MAPbI_3)_x$ films (x = 0−1) including grain size and surface roughness were characterized using scanning electron microscopy (SEM) and atomic-force microscopy (AFM). We find that the film morphology is correlated with the x value (Pb:Sn molar ratio). The SEM images shown in Figure S1 reveal the morphology evolution of mixed Sn−Pb thin films with the change in x. The pure $FASnI_3$ thin film (x = 0) contains some large grains but also more small grains (Figure 1b). The film exhibits a surface root-mean-square (RMS) roughness of 14.8 nm as measured by AFM (Figure S2a). The pure $MAPbI_3$ thin film (x = 1) contains many large grains but with some small ones (Figure 1c). The RMS roughness measured from AFM image (Figure S2c) is 9.5 nm. The $(FASnI_3)_{0.6}(MAPbI_3)_{0.4}$ film contains relatively smaller grains, but with more uniform distribution of grain size (Figure 1d). The surface roughness measured by AFM is only 6.8 nm (Figure S2b), which is smoother than those of pure $FASnI_3$ and $MAPbI_3$ films. The substrate is fully covered with dense grains without any visible pinholes, which is a prerequisite for fabricating efficient thin film solar cells.

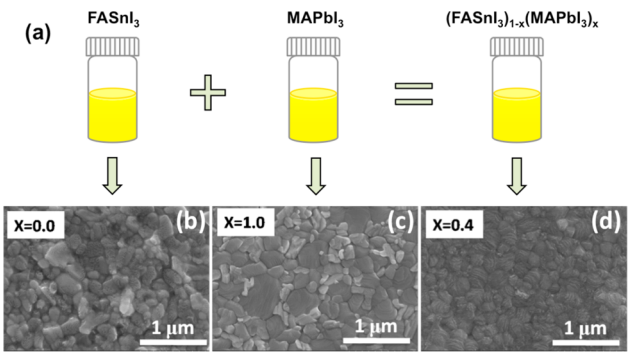

Figure 1. (a) Schematic view of the formation of $(FASnI_3)_{1-x}(MAPbI_3)_x$ precursor. (b, c, d) SEM images of $(FASnI_3)_{1-x}(MAPbI_3)_x$ perovskite thin films with x = 0.0, 1.0, and 0.4.

We characterized the structural and optical properties of $(FASnI_3)_{1-x}(MAPbI_3)_x$ thin films by X-ray diffraction (XRD), Ultraviolet−visible (UV−vis) spectroscopy, photoluminescence (PL), and spectroscopic ellipsometry (SE). As shown in Figure 2a, XRD peak intensities increase as the x value increases, indicating the dependence of film crystallinity on the Pb content. The pure $FASnI_3$ thin film exhibits the poorest crystallinity after annealing at 100 °C. $FASnI_3$ has an orthorhombic ($Amm2$) crystal structure,[8,9,12] whereas $MAPbI_3$ has a tetragonal ($I4\ cm$) crystal structure (β-phase).[3b] It is shown from the XRD patterns in Figure 2a that all mixed Sn−Pb perovskites adopt the orthorhombic crystal structure: the XRD pattern show only one peak within the 2θ range between 22° and 25° (patterns plotted in logarithm scale are shown in Figure S3), which could be indexed to (113) plane in the

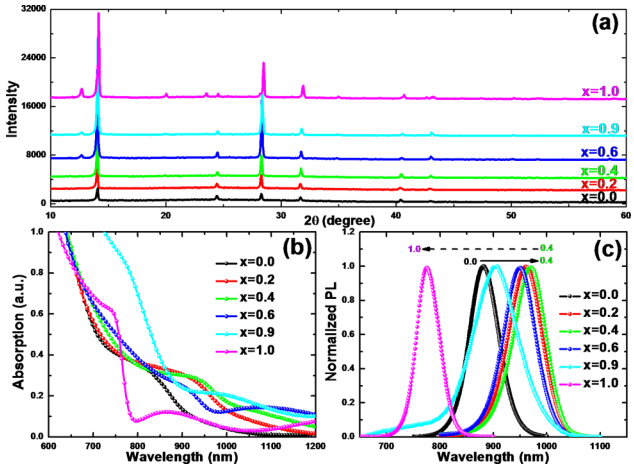

Figure 2. (a) XRD patterns, (b) absorption spectra, and (c) normalized PL spectra of $(FASnI_3)_{1-x}(MAPbI_3)_x$ perovskites with x = 0.0, 0.2, 0.4, 0.6, 0.9, and 1.0.

DOI: 10.1021/jacs.6b08337
J. Am. Chem. Soc. 2016, 138, 12360−12363

*Amm*2 space group. Only the XRD pattern of $MAPbI_3$ (x = 1) shows two peaks within the 2θ range of 22°− 25°, which could be indexed to (211) and (202) planes in the tetragonal *I*4 *cm* space group. The XRD patterns suggest that Sn and Pb randomly occupy the metal sites of corner-sharing octahedra. This is different from the $MASn_{1-x}Pb_xI_3$ perovskites reported by Kanatzidis' group in which only perovskites with low x values (x < 0.5) would adopt the crystal structure of $MASnI_3$ (*P*4 *mm*).[3b] X-ray photoemission spectroscopy analysis (XPS) (Figure S4) indicates that the film compositions are very close to the nominal compositions of their corresponding precursors, indicating a low loss of Sn during film deposition and annealing. UV−vis absorbance spectra (Figure 2b) show that the absorption onsets of all mixed Sn−Pb perovskites are at wavelengths longer than those of $FASnI_3$ and $MAPbI_3$. As the x value increases, the absorption onset first shifts to longer wavelength, reaches a maximum value, and then shifts back to shorter wavelength. The trend of bandgap change as a function of x value has been further confirmed by PL emission peaks shown in Figure 2c and SE shown in Figure S5. It is noted that PL emission peaks can be at shorter wavelengths as compared to the absorption onsets measured from the same samples.[13] The maximum wavelength, which corresponds to a bandgap of ~1.2 eV, is obtained with x = 0.4, giving a composition of $(FASnI_3)_{0.6}(MAPbI_3)_{0.4}$. This bandgap is also confirmed by the external quantum efficiency (EQE) of solar cells using $(FASnI_3)_{0.6}(MAPbI_3)_{0.4}$ absorber (see later discussion). This variation in bandgap is similar to that of the $MASn_{1-x}Pb_xI_3$ perovskite system reported by Kanatzidis' group.[3a,b] It is noted that the smallest bandgap of ~1.2 eV for $(FASnI_3)_{1-x}(MAPbI_3)_x$ perovskites is about 30 meV larger than the smallest bandgap of the $MASn_{1-x}Pb_xI_3$ perovskites (~1.17 eV). This could be due to the inclusion of FA cations in our mixed Sn−Pb perovskites.

The above optical measurements indicate that $(FASnI_3)_{0.6}(MAPbI_3)_{0.4}$ has the lowest bandgap and therefore is the best choice for low-bandgap cell fabrication. We have also conducted time-resolved photoluminescence (TRPL) measurements to determine carrier lifetime of $(FASnI_3)_{1-x}(MAPbI_3)_x$ perovskites with x = 0.0, 0.4, and 1.0, which is an important photovoltaic parameter correlating to the device performance. As shown in Figure 3a and Table S2, the carrier lifetime is 6.7

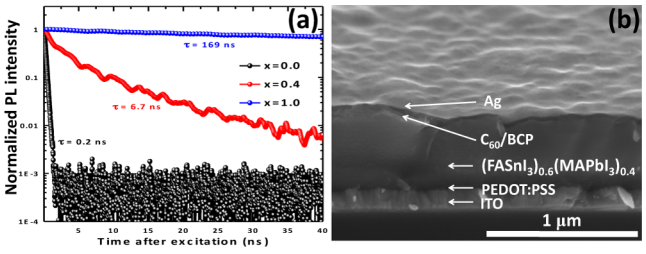

Figure 3. (a) Time-resolved photoluminescence (TRPL) decay of $(FASnI_3)_{1-x}(MAPbI_3)_x$ perovskites with x = 0, 0.4, and 1. (b) Cross-sectional SEM image of our entire device with $(FASnI_3)_{0.6}(MAPbI_3)_{0.4}$ as absorbers, in which each layer is labeled.

ns for $(FASnI_3)_{0.6}(MAPbI_3)_{0.4}$, which is much longer than that of the $FASnI_3$ thin film (0.2 ns), but much shorter than that of the $MAPbI_3$ thin film (169 ns).

Using the inverted planar cell structure, we have successfully fabricated efficient low-bandgap perovskite solar cells using $(FASnI_3)_{0.6}(MAPbI_3)_{0.4}$ as absorbers. The perovskite layers were deposited by spin-coating the precursor on poly(3,4-ethylenedioxythiophene):polystyrenesulfonate (PEDOT:PSS) coated indium tin oxide (ITO) substrates. Figure 3b shows a cross-sectional SEM image of a finished inverted planar $(FASnI_3)_{0.6}(MAPbI_3)_{0.4}$ PVSC with a structure of ITO/PEDOT:PSS/$(FASnI_3)_{0.6}(MAPbI_3)_{0.4}$/$C_{60}$/BCP/Ag. The PEDOT:PSS serves as an HSL, which facilitates hole transfer from the perovskite to the ITO electrode. The C60 serves as an electron selective layer (ESL) that blocks holes and promotes electron transfer.[1d,12] Currently, we do not know the exact band edge positions of $(FASnI_3)_{1-x}(MAPbI_3)_x$ perovskites. We are not able to obtain consistent results using UV photemission spectroscopy (UPS) measurements. The facile oxidation of Sn^{2+} to Sn^{4+} could easily alter the electronic properties of the surfaces and affect the UPS measurement. In fact, the work functions of Sn-based perovskites reported in literature have shown rather inconsistent values.[3b,14]

Figure 4a shows the photocurrent−voltage (J−V) curves of our best performing low-bandgap PVSC using (FAS-

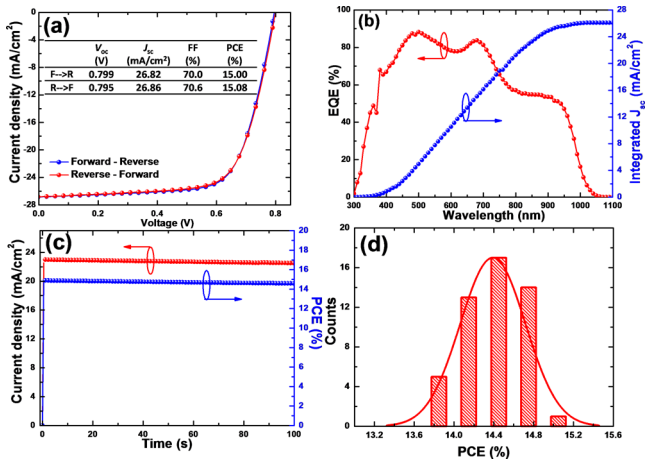

Figure 4. (a) J−V curves under 100 mW/cm^2 AM1.5G illumination measured under reverse and forward voltage scans; (b) EQE and integrated J_{sc}; (c) steady state photocurrent and PCE at a constant bias of 0.648 V, of our best-performing low-bandgap solar cell using $(FASnI_3)_{0.6}(MAPbI_3)_{0.4}$ as absorber. (d) Histograms of PCEs measured for 50 cells using $(FASnI_3)_{0.6}(MAPbI_3)_{0.4}$ absorbers.

$nI_3)_{0.6}(MAPbI_3)_{0.4}$ absorbers measured under different voltage scan directions. This cell has achieved a PCE of 15.08 (15.00)% with a V_{oc} of 0.795 (0.799) V, a J_{sc} of 26.86 (26.82) mA/cm^2, and an FF of 70.6 (70.0)% measured under forward (reverse) voltage scan, exhibiting very small J−V hysteresis behavior, which is ascribed to the complete coverage of perovskite layer, the use of fullerene, and the inverted device architecture.[12] The small J−V hysteresis has been further confirmed by J−V measurements using reverse and forward voltage scans with various scan rates. As shown in Table S1, the scan rate does not significantly affect the PCEs of the cells. Figure 4b shows the EQE spectrum and its corresponding integrated J_{sc} over a 100 mW/cm^2 AM1.5G solar spectrum for this cell. The EQE-integrated J_{sc} can reach 26.08 mA/cm^2, in good agreement with the J_{sc} obtained from the J−V curve. The EQE spectrum shows a spectral response of up to 1030 nm (i.e., approximately 1.2 eV), which is consistent with the bandgap measured from the absorption onset of $(FASnI_3)_{0.6}(MAPbI_3)_{0.4}$ thin films (Figure 2b). To evaluate the actual performance under device operation conditions, we conducted a steady-state performance measure-

DOI: 10.1021/jacs.6b08337
J. Am. Chem. Soc. 2016, 138, 12360−12363

ment. As shown in Figure 4c, the steady-state photocurrent measured at a constant bias of 0.648 V for 100 s under a 100 mW/cm^2 AM1.5G illumination is approximately 22.86 mA/cm^2, corresponding to a stabilized output power of ∼14.8%. The steady-state efficiency is close to the PCE from $J-V$ curves. Compared to the record PCE of 7.37% for the mixed Sn−Pb perovskite cell with a similarly low bandgap achieved by Hao et al.,[3b] the PCE of our best-performing cell represnts a significant advance. We have fabricated 50 devices using $(FASnI_3)_{0.6}(MAPbI_3)_{0.4}$ absorbers in several batches. The cells showed very good reproducibility, as indicated by the PCE histogram shown in Figure 4d. These 50 cells showed an average PCE of 14.39 ± 0.33% with an average V_{oc} of 0.800 ± 0.009 V, an average J_{sc} of 26.33 ± 0.37 mA/cm^2, and an average FF of 68.3 ± 1.2% measured under forward voltage scan, indicating a good reprodicibility.

In summary, we have developed a new precursor combining a $FASnI_3$ precursor with a $MAPbI_3$ precursor. This new precursor enabled us to deposit high quality mixed Sn−Pb perovskite thin films with low bandgaps and to fabricate efficient low-bandgap mixed Sn−Pb perovskite solar cells in the inverted cell structure. The best-performing cell using an absorber with a bandgap of ∼1.2 eV has achieved a PCE higher than 15%. This PCE is significantly higher than the previous record of perovskite solar cells with a similar bandgap. The low bandgap, high efficiency, and high reproducibility represent one significant step toward the realization of efficient all-perovskite tandem solar cells.

■ ASSOCIATED CONTENT

Supporting Information

The Supporting Information is available free of charge on the ACS Publications website at DOI: 10.1021/jacs.6b08337.

Experimental method and additional figures and tables (PDF)

■ AUTHOR INFORMATION

Corresponding Authors

*D.Z. dewei.zhao@utoledo.edu
*R.-G.X. xiongrg@seu.edu.cn
*Y.Y. yanfa.yan@utoledo.edu

Author Contributions

#W.L. and D.Z. contributed equally to this work.

Notes

The authors declare no competing financial interest.

■ ACKNOWLEDGMENTS

This work is financially supported by the U.S. Department of Energy (DOE) SunShot Initiative under the Next Generation Photovoltaics 3 program (DE-FOA-0000990), National Science Foundation under contract no. CHE−1230246 and DMR−1534686, and the Ohio Research Scholar Program. The work at the National Renewable Energy Laboratory is supported by the U.S. Department of Energy SunShot Initiative under the Next Generation Photovoltaics 3 program (DE-FOA-0000990) under Contract No. DE-AC36-08-GO28308. This research used the resources of the Ohio Supercomputer Center and the National Energy Research Scientific Computing Center, which is supported by the Office of Science of the U.S. Department of Energy under Contract No. DE-AC02-05CH11231. The work at Southeast University (P. R. China) is supported by National Natural Science Foundation of China (NSFC) under Contract No. 91422301 and 21427801.

■ REFERENCES

(1) (a) Kojima, A.; Teshima, K.; Shirai, Y.; Miyasaka, T. *J. Am. Chem. Soc.* **2009**, *131* (17), 6050−6051. (b) Ahn, N.; Son, D.-Y.; Jang, I.-H.; Kang, S. M.; Choi, M.; Park, N.-G. *J. Am. Chem. Soc.* **2015**, *137* (27), 8696−8699. (c) Yang, W. S.; Noh, J. H.; Jeon, N. J.; Kim, Y. C.; Ryu, S.; Seo, J.; Seok, S. I. *Science* **2015**, *348*, 1234−1237. (d) Zhao, D.; Sexton, M.; Park, H.-Y.; Baure, G.; Nino, J. C.; So, F. *Adv. Energy Mater.* **2015**, *5* (6), 1401855.

(2) McMeekin, D. P.; Sadoughi, G.; Rehman, W.; Eperon, G. E.; Saliba, M.; Hörantner, M. T.; Haghighirad, A.; Sakai, N.; Korte, L.; Rech, B.; Johnston, M. B.; Herz, L. M.; Snaith, H. J. *Science* **2016**, *351* (6269), 151−155.

(3) (a) Stoumpos, C. C.; Malliakas, C. D.; Kanatzidis, M. G. *Inorg. Chem.* **2013**, *52* (15), 9019−9038. (b) Hao, F.; Stoumpos, C. C.; Chang, R. P. H.; Kanatzidis, M. G. *J. Am. Chem. Soc.* **2014**, *136* (22), 8094−8099. (c) Im, J.; Stoumpos, C. C.; Jin, H.; Freeman, A. J.; Kanatzidis, M. G. *J. Phys. Chem. Lett.* **2015**, *6* (17), 3503−3509.

(4) (a) Bailie, C. D.; Christoforo, M. G.; Mailoa, J. P.; Bowring, A. R.; Unger, E. L.; Nguyen, W. H.; Burschka, J.; Pellet, N.; Lee, J. Z.; Gratzel, M.; Noufi, R.; Buonassisi, T.; Salleo, A.; McGehee, M. D. *Energy Environ. Sci.* **2015**, *8* (3), 956−963. (b) Kranz, L.; Abate, A.; Feurer, T.; Fu, F.; Avancini, E.; Löckinger, J.; Reinhard, P.; Zakeeruddin, S. M.; Grätzel, M.; Buecheler, S.; Tiwari, A. N. *J. Phys. Chem. Lett.* **2015**, *6* (14), 2676−2681. (c) Heo, J. H.; Im, S. H. *Adv. Mater.* **2016**, *28* (25), 5121−5125. (d) Liu, J.; Lu, S.; Zhu, L.; Li, X.; Choy, W. C. H. *Nanoscale* **2016**, *8* (6), 3638−3646.

(5) (a) Zhao, Y.; Zhu, K. *J. Am. Chem. Soc.* **2014**, *136* (35), 12241−12244. (b) Bi, C.; Yuan, Y.; Fang, Y.; Huang, J. *Adv. Energy Mater.* **2015**, *5* (6), 1401616.

(6) Zuo, F.; Williams, S. T.; Liang, P.-W.; Chueh, C.-C.; Liao, C.-Y.; Jen, A. K. Y. *Adv. Mater.* **2014**, *26* (37), 6454−6460.

(7) Yang, Z.; Rajagopal, A.; Chueh, C.-C.; Jo, S. B.; Liu, B.; Zhao, T.; Jen, A. K. Y. *Adv. Mater.* **2016**, DOI: 10.1002/adma.201602696.

(8) Koh, T. M.; Krishnamoorthy, T.; Yantara, N.; Shi, C.; Leong, W. L.; Boix, P. P.; Grimsdale, A. C.; Mhaisalkar, S. G.; Mathews, N. *J. Mater. Chem. A* **2015**, *3* (29), 14996−15000.

(9) Lee, S. J.; Shin, S. S.; Kim, Y. C.; Kim, D.; Ahn, T. K.; Noh, J. H.; Seo, J.; Seok, S. I. *J. Am. Chem. Soc.* **2016**, *138* (12), 3974−3977.

(10) (a) Chung, I.; Lee, B.; He, J.; Chang, R. P. H.; Kanatzidis, M. G. *Nature* **2012**, *485* (7399), 486−489. (b) Kumar, M. H.; Dharani, S.; Leong, W. L.; Boix, P. P.; Prabhakar, R. R.; Baikie, T.; Shi, C.; Ding, H.; Ramesh, R.; Asta, M.; Graetzel, M.; Mhaisalkar, S. G.; Mathews, N. *Adv. Mater.* **2014**, *26* (41), 7122−7127.

(11) Ke, W.; Xiao, C.; Wang, C.; Saparov, B.; Duan, H.-S.; Zhao, D.; Xiao, Z.; Schulz, P.; Harvey, S. P.; Liao, W.; Meng, W.; Yu, Y.; Cimaroli, A. J.; Jiang, C.-S.; Zhu, K.; Al-Jassim, M.; Fang, G.; Mitzi, D. B.; Yan, Y. *Adv. Mater.* **2016**, *28*, 5214−5221.

(12) Liao, W.; Zhao, D.; Yu, Y.; Grice, C. R.; Wang, C.; Cimaroli, A. J.; Schulz, P.; Meng, W.; Zhu, K.; Xiong, R.-G.; Yan, Y. *Adv. Mater.* **2016**, DOI: 10.1002/adma.201602992.

(13) Dong, Q.; Fang, Y.; Shao, Y.; Mulligan, P.; Qiu, J.; Cao, L.; Huang, J. *Science* **2015**, *347* (6225), 967−970.

(14) (a) Ogomi, Y.; Morita, A.; Tsukamoto, S.; Saitho, T.; Fujikawa, N.; Shen, Q.; Toyoda, T.; Yoshino, K.; Pandey, S. S.; Ma, T.; Hayase, S. *J. Phys. Chem. Lett.* **2014**, *5* (6), 1004−1011. (b) Wang, F.; Ma, J.; Xie, F.; Li, L.; Chen, J.; Fan, J.; Zhao, N. *Adv. Funct. Mater.* **2016**, *26* (20), 3417−3423.

DOI: 10.1021/jacs.6b08337
J. Am. Chem. Soc. 2016, 138, 12360−12363